ISBN: 978-3-95450-220-2 ISSN: 2673-5474 doi: 10.18429/JACoW-FEL2022-TUP44

PHASE-LOCKED HARD X-RAY SELF-SEEDING FEL STUDY FOR THE EUROPEAN XFEL

T. Long[1], S. Huang, K. Liu
State Key Laboratory of Nuclear Physics and Technology, Peking University, Beijing, China
Y. Chen, W. Decking, S. Liu*, N. Mirian, W. Qin
Deutsches Elektronen-Synchrotron (DESY), Hamburg, Germany
G. Geloni†, J. Yan, European XFEL, Schenefeld, Germany
[1]also at DESY, Hamburg, Germany

Abstract

Phase-locked pulses are important for coherent control experiments. Here we present theoretical analyses and start-to-end simulation results for the generation of phase-locked pulses using the Hard X-ray Self-Seeding (HXRSS) system at the European XFEL. As proposed by Sven Reiche *et al.* in "A perfect X-ray beam splitter and its applications to time-domain interferometry and quantum optics exploiting free-electron lasers", 2022, the method is based on a combination of self-seeding and fresh-slice lasing techniques. However, at variance with this reference, here we exploit different transverse centroid offsets along the electron beam. In this way we may first utilize part of the electron beam to produce SASE radiation, to be filtered as seed and then generate HXRSS pulses from other parts of the beam applying appropriate transverse kicks. The final result consists in coherent radiation pulses with fixed phase difference and tunable time delay within the bunch length. This scheme can be useful for coherent control applications such as coherent x-ray pump-probe experiments.

INTRODUCTION

Phase-locking means a fixed phase relation between successive pulses [1] and phase-locked pulses are important for coherent control experiments [2–4]. Usually a split-and-delay scheme is employed to generate phase-locked pulses in the optical to the extreme ultraviolet wavelengths, while it is challenging to produce phase-locked pulses down to the X-ray regime. X-ray free-electron lasers (FELs) deliver photon pulses with extremely high intensity and show remarkable capabilities for researches in physics, chemistry and biology [5,6]. Self-seeding schemes [7–10] can provide nearly fully coherent x-ray FELs and expand their application to a broader range [11]. Several methods have been proposed to generate coherent phase-locked X-ray pulses from externally seeded FELs [12–15] or using self-seeding techniques [16]. In the first case, the achievable wavelength is limited within the soft x-ray spectral region typical of the high gain harmonic generation configuration, while the second scheme can operate in both soft and hard X-ray regimes by properly choosing the self-seeding monochromators. In Ref. [16], the employed method is based on a combination of self-seeding and fresh-slice lasing techniques and can offer much higher phase stability than conventional X-ray split-and-delay approaches.

Here we present theoretical analyses and start-to-end simulation results for the generation of phase-locked pulses using the Hard X-ray Self-Seeding (HXRSS) system at the European XFEL. European XFEL is an X-ray FEL facility based on a superconducting linear accelerator [17]. After the collimation section that follows the main linac, there is an arc [18, 19] that bends selected electron beams from a bunch train to the hard x-ray FEL beamline SASE2, where the HXRSS system is built [20]. There are 35 undulator segments of 5 m length interspaced by 1.1 m sections with magnets elements. For the HXRSS system, two single crystal monochromators and chicanes are installed in two positions: one between 8th and 9th segments, the other one between 16th and 17th segments. This configuration provides the flexibility to increase spectrum signal-to-noise ratio by choosing one- or two-chicane scheme according to difference photon energies, and to mitigate crystal heat load effect by using two-chicane scheme for lower photon energies [20].

At variance with Ref. [16], where different lasing parts of the electron beam are defined by the slotted foil in a dispersion section, here we exploit different transverse centroid offsets along the electron beam. This offsets may be induced by collective coherent synchrotron radiation (CSR) effects [21,22] during the beam transport in the arc upstream of the SASE2 undulators. The method proposed here does not suffer from possible limitation on the beam repetition rate, while the spoiler technique employing slotted foil may do due to radiation losses [23]. In this way we may first utilize part of the electron beam to produce SASE radiation, which is monochromatized as coherent seed to trigger seeded lasing with other parts of the beam that are appropriately kicked on the undulator axis. The final result consists in phase-locked coherent radiation pulses with tunable time delay within the bunch length.

In the following, we will first introduce the slice centroid deviation based scheme to generate phase-locked HXRSS FEL, then CSR effect in the arc before SASE2 at the European XFEL is analysed. Finally the start-to-end simulation is presented.

* shan.liu@desy.de
† gianluca.aldo.geloni@xfel.eu

ISBN: 978-3-95450-220-2 ISSN: 2673-5474 doi: 10.18429/JACoW-FEL2022-TUP44

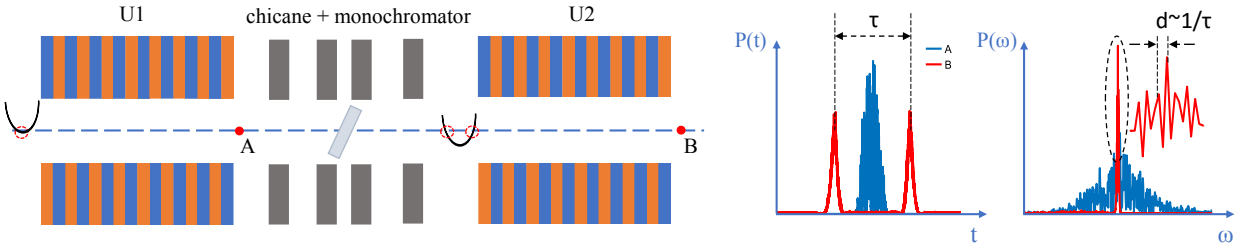

Figure 1: Schematic plot of phase-locked HXRSS FEL generation from electron beam with different slice centroid deviation. In the first undulator U1, the central part of electron beam is kicked on axis (dashed line) and radiate SASE. The SASE pulse is then monochromatized with a Bragg crystal and the electron beam bypasses the monochromator and is realigned with different parts on axis. The delayed electron beam overlaps with the monochromatized seeding wake to generate seeded pulses in the final undulator U2. Different lasing parts of the electron beam are indicated by red dashed circles. Plots on the right are power and spectrum distribution for both SASE and seeded pulses. A and B correspond to positions at the exit of U1 and U2, respectively. An enlarged plot is shown for the central part of the seeded spectrum, as denoted by the black dashed ellipse.

RESULTS

The proposed method for phase-locked HXRSS FEL generation is shown in Fig. 1, where an electron beam with parabolic or V-like shape with different slice centroid deviation is required. Different parts of electron beam lase separately in different stages, as the red dashed circles indicate. In the first stage, central part of electron beam is kicked with magnetic correctors on axis in undulator 1 (U1) for SASE radiation. For efficient interaction between electron beam and FEL pulse, the on-axis lasing part should have a radius approximated as [5] $\sigma_x \sim \sigma_r \sim \sqrt{\lambda_r L_g/(4\pi)}$, where λ_r is the FEL resonant wavelength and L_g the gain length. Other parts of the beam undergo betatron oscillation without lasing due to inefficient overlap with the radiation field, hence beam quality is preserved for these parts.

In the second stage, the SASE pulse is filtered by a single crystal monochromator to generate coherent seeding wake [7] while the electron beam is deflected and delayed by chicane and bypasses the monochromator. In the final stage, electron beam is kicked again with unspoiled parts on axis to overlap with the monochramatized wake to generate seeded lasing in undulator 2 (U2). Delay between the two lasing parts is determined by the kick amount and limited by electron bunch length and quality. The two lasing parts are seeded with the same coherent seed and generated seeded pulses are naturally phase-locked. Radiation power and spectrum are shown for both SASE and seeded lasing at the exit of U1 (A) and U2 (B), respectively. One can see in U1 a single SASE pulse is generated with a broad spectrum, while in U2 coherent twin pulses are generated with a much narrower spectrum. For phase-locked pulses, pulse delay τ in time domain corresponds to the spike distance d in frequency domain, where $d \sim 1/\tau$ and the spike width is inversely proportional to the pulse number (here it's two), as shown in the right plots, where the central part of the seeded spectrum is enlarged in the plugin.

The parabolic or V-like different slice centroid deviation is important for this method to work. Such beam shape can be generated with dispersion-based method [24], where sextupole magnets are placed in the dispersive sections for two-color pulse pairs generation utilizing beams with energy chirp. Here we present initial simulation results to show that it is possible to utilize CSR effect, which is always treated as detrimental in FEL facilities and many methods are proposed to suppress this effect [25, 26].

The desired centroid deviation is introduced through CSR effect, as shown in Fig. 2. Beam head is to the right in all the following figures. The beam transport simulation is carried out with the multi-physics software package OCELOT [27]. An ideal electron beam distribution with electron energy of 14 GeV, beam charge of 250 pC, guassian distribution both in longitudinal and transverse phase space is used as input before the arc, and the arc lattice remains the same with designed dispersion-free optics. It is shown that CSR dominates over other collective effects such as space charge and wakefield influence in the arc [28]. Here among these collective effects only CSR is considered.

The electron beam has a Gaussian current profile with peak value of around 5 kA and FWHM 15 μm. The whole beam slices have nearly zero initial centroid deviation in both transverse direction (Fig. 2(a)). Significant slice centroid deviation is observed after transport through the arc, especially in the horizontal direction x, as shown in Fig. 2(b). Also, energy modulation is induced through the arc, as shown in Fig. 2(c). The modulation process can be understood as that during the transport in the arc, CSR induces energy modulation in the first part of arc, then this energy chirp undergoes dispersion in the last part of arc and results beam centroid deviation at the arc exit. Though the net dispersion of the whole arc is zero, the final part is not. The induced energy chirp and beam centroid deviation is closely related to the beam current profile with a small shift of the maximum modulation position compared to the peak current position.

ISBN: 978-3-95450-220-2 ISSN: 2673-5474 doi: 10.18429/JACoW-FEL2022-TUP44

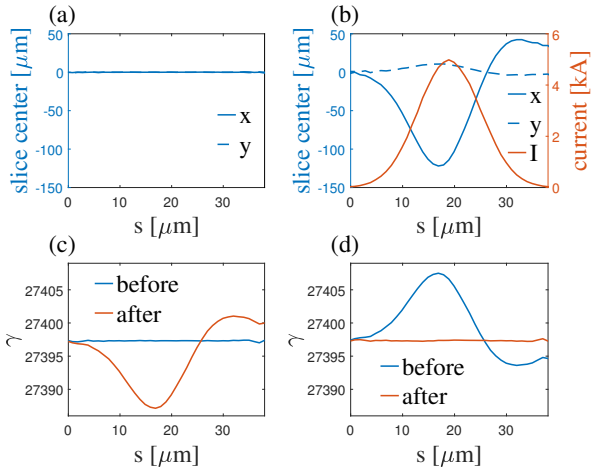

Figure 2: Beam slice properties before and after transport in arc with ideal initial beam distribution at arc entrance. (a) slice center before arc. (b) slice center after arc and beam current profile. (c) slice electron energy (γ) before and after arc. (d) same as (c) with different initial energy distribution.

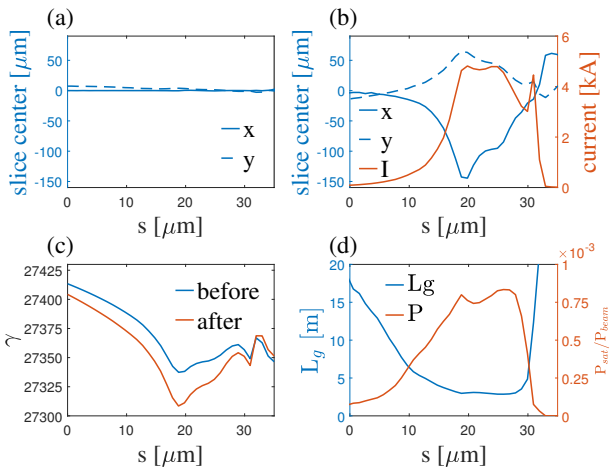

Figure 3: Beam slice properties before and after transport in arc with beam distribution from start-to-end simulation. (a) slice center before arc. (b) slice center after arc and current profile. (c) slice electron energy (γ) before and after arc. (d) theoretical slice gain length and normalized saturation power along the beam at the entrance of the SASE2 undulator beamline.

This shift results in an asymmetric current distribution in the two lasing beam parts in the final seeded lasing stage, which usually results in twin pulses with different power. It is interesting to note that if we use another ideal initial beam distribution with inverse energy modulation of red curve in Fig. 2(c), while other parameters remain the same, then we can get centroid deviated beam as shown in Fig. 2(b) and remove energy chirp as shown in Fig. 2(d) after transport in the arc. This may be beneficial for applications requiring beam centroid deviation while with constant beam energy. Simulations also show that if we turn off CSR effect there will be no energy modulation nor beam centroid deviation after transport in the arc.

Beam properties before and after transport in the arc from start-to-end simulation are shown in Fig. 3. We observe similar centroid deviation and energy modulations as in Fig. 2. Here, the current profile is much more complicated than the ideal Gaussian profile, however, the modulation shape also inherits the current profile with peak modulation position slightly shifted. In Fig. 3(b), horizontal slice centroid deviation at bunch position s=20 µm is x=-145 µm, while at s=17 µm and s=27 µm the two slices have same horizontal deviation of x=-82 µm. The deviation difference is around 63 µm and is larger than the typical transverse lasing width. In the following simulation we first kick slice at position s=20 µm on axis in U1 to radiate SASE then kick slices at s=17 µm and s=27 µm on axis in U2 for seeded lasing.

Beam quality for lasing is shown in Fig. 3(d), where the slice gain length L_g is calculated with Ming Xie's formula [29] and the normalized saturation power $P = P_{sat}/P_{beam}$ is calculated from [30] $P = 1.6\rho(L_{g0}/L_g)^2$ with resonant photon energy of 10 keV, where P_{sat} and P_{beam} are saturated radiation power and beam power, ρ is Pierce parameter, L_{g0} 1D gain length.

FEL lasing process is simulated with GENESIS [31]. We use the start-to-end simulated beam distribution as input at the undulator entrance and single shot simulation results are shown in Fig. 4, with resonant photon energy E_c=10 keV. For the first SASE stage, the gain length is around 3 m and we utilize the first 16 undulator segments, where radiation pulse energy reaches around 340 µJ at the exit of U1, as denoted by point A in Fig. 4(a). SASE power and spectrum are shown in Fig. 4(b) and (c), indicating a single pulse and broad spectrum. A diamond crystal with C(004) reflection and thickness of 100 µm is used to monochromatize the SASE pulse and chicane strength is tuned to delay electron beam by 15 µm to overlap with the seeding wake. The seeded lasing pulse energy increases from several µJ to 70 µJ at point B in the linear gain regime, 320 µJ at point C in saturation regime, and to post saturation with more than 690 µJ. Seeded FEL spectrum at point B is shown in Fig. 4(d). The coherent twin pulses are separated with 10 µm, this delay corresponds to spectrum spike distance of 0.124 eV. The plugin in Fig. 4(d) shows spectrum at [0, 1.24] eV, where one can find exactly 10 spikes in this range, which confirms phase-locking of the coherent twin pulses. However, due to the electron energy and current difference between the two lasing parts, the twin pulses have different power with slightly different central photon energy. The left pulse has lower power and higher photon energy, hence spectrum spikes are only found on the right side. Two spectrum envelopes emerge in saturation regime, as denoted by point C and Fig. 4(e) and (f). The seeded FEL has much narrower spectrum than SASE with FWHM less than 3 eV.

ISBN: 978-3-95450-220-2 ISSN: 2673-5474 doi: 10.18429/JACoW-FEL2022-TUP44

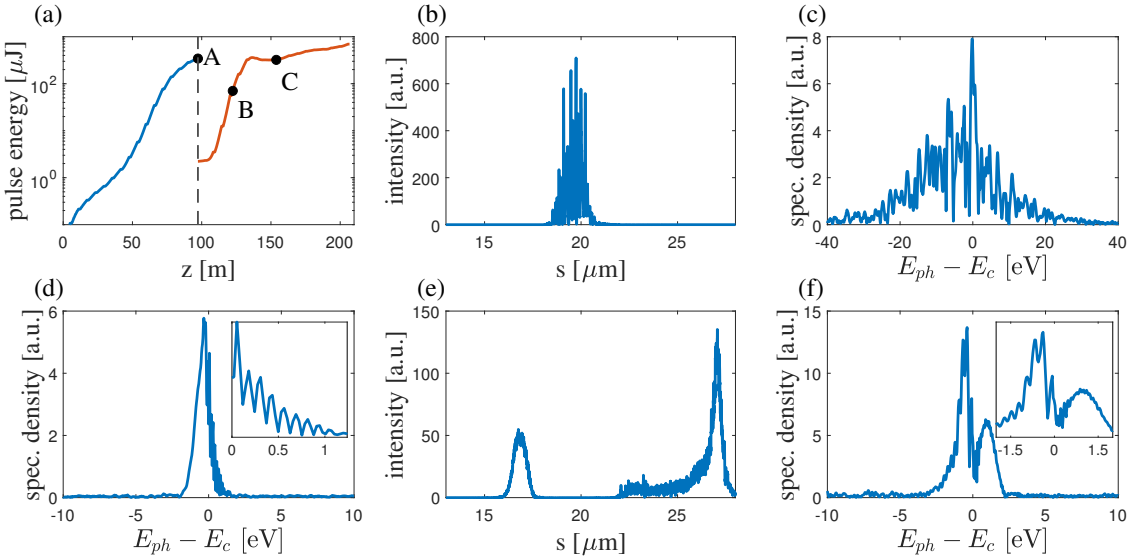

Figure 4: Radiation properties with beam distribution from start-to-end simulation. (a) pulse energy evolution along undulator for first SASE then seeded lasing stages in U1 and U2. (b) and (c) on-axis intensity and spectrum of SASE pulse at position A in (a). (d) on-axis seeded pulse spectrum at position B in (a). (e) and (f) on-axis intensity and spectrum of seeded pulse at position C in (a). The plugins in (d) and (f) show enlarged spectrum center.

CONCLUSION

In summary, a method utilizing different electron beam centroid deviation is proposed to generate phase-locked HXRSS FEL pulses. The centroid deviation can be induced by CSR effects when the beam is transported thorough an arc before the undulator beamline. Different beam parts are steered to lase seperately at different stages. This method is a combination of fresh slice and self-seeding techniques and is naturally suitable for high repetition rate operations. The proposed scheme may well facilitate the coherent x-ray pump-probe experiments.

ACKNOWLEDGEMENTS

We would like to acknowledge helpful discussions with N. Golubeva, S. Tomin and S. Walker. We would also like to thank R. Feidenhans'l for useful discussions and his interest in this work.

REFERENCES

[1] D. Oepts and W. Colson, "Phase locking in an infrared short-pulse free-electron laser", *IEEE J. Quantum Electron.*, vol. 26, no. 4, pp. 723–730, 1990. doi:10.1109/3.53390

[2] B. W. Adams *et al.*, "X-ray quantum optics", *J. Mod. Opt.*, vol. 60, no. 1, pp. 2–21, 2013. doi:10.1080/09500340.2012.752113

[3] S. T. Cundiff and S. Mukamel, "Optical multidimensional coherent spectroscopy", *Phys. Today*, vol. 66, no. 7, pp. 44–49, 2013. doi:10.1063/PT.3.2047

[4] K. Prince *et al.*, "Coherent control with a short-wavelength free-electron laser", *Nat. Photonics*, vol. 10, no. 3, pp. 176–179, 2016. doi:10.1038/nphoton.2016.13

[5] Z. Huang and K.-J. Kim, "Review of x-ray freeelectron laser theory", *Phys. Rev. Spec. Top. Accel Beams*, vol. 10, no. 3, p. 034801, 2007. doi:10.1103/PhysRevSTAB.10.034801

[6] J. C. Spence, U. Weierstall, and H. Chapman, "X-ray lasers for structural and dynamic biology", *Rep. Prog. Phys.*, vol. 75, no. 10, p. 102601, 2012. doi:10.1088/0034-4885/75/10/102601

[7] G. Geloni, V. Kocharyan, and E. Saldin, "A novel self-seeding scheme for hard x-ray FELs", *J. Mod. Opt.*, vol. 58, no. 16, pp. 1391–1403, 2011. doi:10.1080/09500340.2011.586473

[8] J. Amann *et al.*, "Demonstration of self-seeding in a hard-x-ray freeelectron laser", *Nat. Photonics*, vol. 6, no. 10, pp. 693–698, 2012. doi:10.1038/nphoton.2012.180

[9] I. Inoue *et al.*, "Generation of narrow-band x-ray free-electron laser via reflection self-seeding", *Nat. Photonics*, vol. 13, no. 5, pp. 319–322, 2019. doi:10.1038/s41566-019-0365-y

[10] I. Nam *et al.*, "High-brightness self-seeded x-ray free-electron laser covering the 3.5 kev to 14.6 kev range", *Nat. Photonics*, vol. 15, no. 6, pp. 435–441, 2021. doi:10.1038/s41566-021-00777-z

ISBN: 978-3-95450-220-2 ISSN: 2673-5474 doi: 10.18429/JACoW-FEL2022-TUP44

[11] C. Bostedt *et al.*, "Linac coherent light source: The first five years", *Rev. Mod. Phys.*, vol. 88, no. 1, p. 015007, 2016. doi:10.1103/RevModPhys.88.015007

[12] N. Thompson and B. McNeil, "Mode locking in a free-electron laser amplifier", *Phys. Rev. Lett.*, vol. 100, no. 20, p. 203901, 2008. doi:10.1103/PhysRevLett.100.203901

[13] D. Xiang, Y. Ding, T. Raubenheimer, and J. Wu, "Mode-locked multichromatic x rays in a seeded free-electron laser for single-shot x-ray spectroscopy", *Phys. Rev. Spec. Top. Accel Beams*, vol. 15, no. 5, p. 050707, 2012. doi:10.1103/PhysRevSTAB.15.050707

[14] D. Gauthier *et al.*, "Generation of phaselocked pulses from a seeded free-electron laser", *Phys. Rev. Lett.*, vol. 116, no. 2, p. 024801, 2016. doi:10.1103/PhysRevLett.116.024801

[15] A. Wituschek *et al.*, "Tracking attosecond electronic coherences using phase-manipulated extreme ultraviolet pulses", *Nat. Commun.*, vol. 11, no. 1, pp. 1–7, 2020. doi:10.1038/s41467-020-14721-2

[16] S. Reiche, G. Knopp, B. Pedrini, E. Prat, G. Aeppli, and S. Gerber, "A perfect x-ray beam splitter and its applications to time-domain interferometry and quantum optics exploiting free-electron lasers", *PNAS*, vol. 119, no. 7, p. e2117906119, 2022. doi:10.1073/pnas.2117906119

[17] W. Decking *et al.*, "A MHz-repetition-rate hard X-ray free-electron laser driven by a superconducting linear accelerator", *Nat. Photonics*, vol. 14, no. 6, pp. 391–397, 2020. doi:10.1038/s41566-020-0607-z

[18] W. Decking and F. Obier, "Layout of the beam switchyard at the European XFEL", *EPAC08-WEPC073*, Genoa, Italy, 2008.

[19] N. Golubeva, V. Balandin, and W. Decking, "Optics for the Beam Switchyard at the European XFEL", in *Proc. IPAC'11*, San Sebastian, Spain, Sep. 2011, paper WEPC008, pp. 2016–2018.

[20] S. Liu *et al.*, "Preparing for high-repetition rate hard x-ray self-seeding at the European x-ray free electron laser: Challenges and opportunities", *Phys. Rev. Accel. Beams*, vol. 22, no. 6, p. 060704, 2019. doi:10.1103/PhysRevAccelBeams.22.060704

[21] E. L. Saldin, E. A. Schneidmiller, and M. Yurkov, "Radiative interaction of electrons in a bunch moving in an undulator", *Nucl. Instrum. Methods Phys. Res., Sect. A*, vol. 417, no. 1, pp. 158–168, 1998. doi:10.1016/S0168-9002(98)00623-8

[22] M. Dohlus, "Two methods for the calculation of CSR fields", *CM-P00048519, Tech. Rep.*, 2003.

[23] A. Potter *et al.*, "Investigation of the beam losses and radiation loads for the implementation of a slotted foil in the European XFEL", *40th Free Electron Laser Conf.*, vol. WEP16, 2022.

[24] P. Dijkstal, A. Malyzhenkov, S. Reiche, and E. Prat, "Demonstration of two-color x-ray free-electron laser pulses with a sextupole magnet", *Phys. Rev. Accel. Beams*, vol. 23, no. 3, p. 030703, 2020. doi:10.1103/PhysRevAccelBeams.23.030703

[25] V. Yakimenko, M. Fedurin, V. Litvinenko, A. Fedotov, D. Kayran, and P. Muggli, "Experimental observation of suppression of coherent-synchrotron-radiation–induced beam-energy spread with shielding plates", *Phys. Rev. Lett.*, vol. 109, no. 16, p. 164802, 2012. doi:10.1103/PhysRevLett.109.164802

[26] S. Di Mitri, M. Cornacchia, and S. Spampinati, "Cancellation of coherent synchrotron radiation kicks with optics balance", *Phys. Rev. Lett.*, vol. 110, no. 1, p. 014801, 2013. doi:10.1103/PhysRevLett.110.014801

[27] I. Agapov, G. Geloni, S. Tomin, and I. Zagorodnov, "Ocelot: A software framework for synchrotron light source and fel studies", *Nuclear Instruments and Methods in Physics Research Section A: Accelerators, Spectrometers, Detectors and Associated Equipment*, vol. 768, pp. 151–156, 2014. doi:10.1016/j.nima.2014.09.057

[28] I. Zagorodnov, "Beam dynamics in sase2 arc", 2019.

[29] M. Xie, "Exact and variational solutions of 3D eigenmodes in high gain FELs", *Nucl. Instrum. Methods Phys. Res., Sect. A*, vol. 445, no. 1-3, pp. 59–66, 2000. doi:10.1016/S0168-9002(00)00114-5

[30] K.-J. Kim and M. Xie, "Self-amplified spontaneous emission for short wavelength coherent radiation", *Nucl. Instrum. Methods Phys. Res., Sect. A*, vol. 331, no. 1-3, pp. 359–364, 1993. doi:10.1016/0168-9002(93)90072-P

[31] S. Reiche, "Genesis 1.3: a fully 3d time-dependent FEL simulation code", *Nucl. Instrum. Methods Phys. Res., Sect. A*, vol. 429, no. 1-3, pp. 243–248, 1999. doi:10.1016/S0168-9002(99)00114-X